AIChE WILEY InterScience DISCOVER SOMETHING GREAT

SEPARATIONS

The Impact of Valve Tray Geometry on the Interfacial Area of Mass Transfer

Yin-Chun Liang, Zheng Zhou, Min Shao, Jiao Geng, You-Ting Wu, and Zhi-Bing Zhang
Separation Engineering Research Center (SERC), School of Chemistry and Chemical Engineering, Nanjing University, Nanjing, 210093, P.R. China

DOI 10.1002/aic.11489
Published online April 18, 2008 in Wiley InterScience (www.interscience.wiley.com).

The interfacial area of mass transfer is one of the key parameters in valve tray design, and the valve geometry is the important structural parameter that determines the interfacial area. In this work, the hydrodynamic and mass-transfer characteristics of three different types of valve trays are investigated. The mechanism of bubbles deformation and breakage in the turbulent dispersion system is theoretically analyzed on the basis of Kolmogoroff's isotropic turbulence hypothesis, and a novel model is proposed to predict the interfacial area. The results show that the simulation results agree well with the experimental data. In contrast to most of the conventional models, the present model is capable of evaluating the effects of valve configuration on the interfacial area. The model is expected to guide effectively the design of valve trays which is widely applied nowadays.
 AIChE J, 54: 1470–1477, 2008
Keywords: interfacial area, bubble, valve tray, Kolmogoroff's isotropic turbulence hypothesis

Introduction

One of the major tasks in the design of separation processes is to simulate separation processes accurately. Nowadays the nonequilibrium model has been popularly used to realize the simulation, in which the interfacial area is a key parameter. The valve trays, being the topic of our article, are among the most widely employed equipments in tray columns, and its valve geometry becomes the determined factor for the interfacial area of mass transfer. Developed through the past decades, new-style valves with different geometries have been invented for the purpose of improving tray performance, especially separation efficiency. Although column design procedures are generally considered as "mature," information for the design of modern valve trays is still quite scarce. Since the design of most modern valves is mainly based on experience, being lack of theoretical research, the accurate simulation of separation processes becomes difficult. To our knowledge, only Richard et al.[1] reported the mass transfer characteristics of valve trays using dimensional analysis to obtain an empirical expression for the interfacial area. In addition, only V-1 type valve was investigated, and the mechanism of the interface formation had not been theoretically analyzed in their work. Till recent years, some researchers[2–4] analyzed the mechanism of interface formation from the relations among bubble hydrodynamics, system property, and operation conditions, and advanced some strict models that have been developed to predict the interfacial area. However, there are none of theoretical models that are especially applicable to the valve trays. In particular, the impact of valve geometry on the interfacial area still cannot be expressed using an available correlation. Therefore, the main objective of the present work is to analyze the functioning mechanism of valve geometry on the interfacial area, and derive an appropriate correlation.

Theoretical section

At high superficial velocity of the vapor, a turbulent flow pattern dominates the liquid phase flowing on the valve tray. It is very difficult to predict theoretically the interfacial area

Correspondence concerning this article should be addressed to Z.-B. Zhang or Y.-T. Wu at segz@nju.edu.cn.

due to the randomicity and complexity of the turbulent motion. Fortunately, the mechanism of bubble deformation and breakage can be employed to analyze the turbulent flow, provided that the Kolmogoroff's isotropic turbulence hypothesis[5] can be used. When the vapor is sparged into the liquid, a series of different length scale eddies are created from the liquid being stirred. The large eddies, being nonisotropic and unsteady, can break easily to be the small eddies that behave to be isotropic. Most of the turbulent energy is dissipated by the small eddies, but not the large ones. All these ideas become the theoretical basis of the Kolmogoroff's isotropic turbulence hypothesis. When this theory is applied to the bubble columns, difficulties in obtaining analytical solution for the crowded bubbles can be therefore avoided using the energy dissipation rate ε to describe the properties of the vapor and liquid.

Energy dissipation rate on the valve tray

In the turbulent dispersion system, Hean et al. assumed that only these eddies having the length scale smaller than or equal to the bubble diameter could participate in the deformation of bubbles, whereas those having length scale larger than the bubble diameter mainly converted the bubbles.[6] In this work, such assumption is also used, together with the Kolmogoroff's isotropic turbulence theory. Now that most of the turbulent energy is dissipated by these small eddies, a part of the turbulent energy may be converted to heat energy through viscous dissipation, whereas the other part may contribute to surface energy during the bubble deformation. With the aid of the assumptions above, the description of kinetic characteristics of bubbles can be greatly simplified by introducing the energy dissipation rate ε.

The energy dissipation rate on the valve tray, quantitatively equal to the input energy rate from vapor to liquid, is associated with the hydrodynamic characteristic of the valve tray. When the vapor passes through the liquid, the pressure drop ΔP_{L} can be expressed as

$$\Delta P_{\mathrm{L}} = \rho_{\mathrm{L}} g h_{\mathrm{L}} \tag{1}$$

where h_{L} is the clear liquid height, and the liquid mass per tray area can be defined as $\rho_{\mathrm{L}} h_{\mathrm{L}}$. As calculated from the nonequilibrium thermodynamic model, the entropy generation rate due to the temperature gradient is very small in the whole energy dissipation, it is reasonable to neglect the energy dissipation due to the temperature gradient.[7] The energy dissipation rate per tray area can thus be obtained as

$$\Delta E_{\mathrm{L}} = \Delta P_{\mathrm{L}} u_{\mathrm{G}} \tag{2}$$

where u_{G} is the superficial velocity of the vapor. Since the major part of the energy loss comes from overcoming the hydrostatic head of the liquid layer,[8] the rest part of the energy loss contributes to the increase of turbulent energy of the liquid and can be defined as $C_d \Delta E_{\mathrm{L}}$. The energy dissipation rate for the liquid of unit mass is consequently written as

$$\varepsilon = \frac{C_d \Delta E_{\mathrm{L}}}{\rho_{\mathrm{L}} h_{\mathrm{L}}} \tag{3}$$

where $0 < C_d < 1$ is the energy dissipation percentage that is dependent on the tray configurations. C_d has different values for various valve geometries, despite the fact that for all kinds of valve trays the vapor jets out from valve slots. Two key parameters have crucial influence on C_d: the slot angle and the slot area. The slot angle mainly controls the initial flow-directions of bubbles in the liquid layer, and its influence on the bubble size is negligible. However, the slot area, being product of the effective slot perimeter l and slot height h, can greatly affect the contact area of the vapor and liquid. The larger slot area can provide the larger contact area and the longer contact time for the vapor and liquid, leading to the increase of the energy exchanges between the vapor and liquid. As a result, the input energy from the vapor to the liquid, being equal to the energy dissipation rate for unit liquid mass, is also enhanced. Dimensional analysis can be applied to give an equation of the form

$$C_d = C_1 \left(\frac{nlh}{A_{\mathrm{b}}} \right)^{C_2} \tag{4}$$

where C_1 and C_2 are the two regression coefficients to be determined, n is the valve number per tray, and A_{b} is the bubble area of the tray. Substituting Eqs. 1, 2, and 4 into Eq. 3, generates Eq. 5,

$$\varepsilon = C_1 \left(\frac{nlh}{A_{\mathrm{b}}} \right)^{C_2} u_{\mathrm{G}} g \tag{5}$$

Vapor-liquid interfacial area

The interfacial area is mainly determined by the bubble size at a definite vapor flow rate. Lots of research efforts have been put on establishing methods to estimate the bubble size, especially the maximum stable bubble size. In the turbulent dispersion system, it is commonly believed that more than one mechanism for bubble breakage may exist. This is because a bubble is not only exposed to a turbulent field, but also subjected to both inertial and viscous forces. Normally, the turbulent breakage and viscous shear breakage are considered to be the most important.[6] However, when bubble breakage under highly turbulent flow is considered, the viscous forces may usually be neglected owing to the fact that the sizes of bubbles are usually much larger than those of the turbulence. The turbulent breakage is generally induced by eddies bombarding and deforming the bubble surface. Only a certain number of bubble-eddy collision are likely to result in bubble crushing, and the break up of bubbles is determined by the equilibrium between the inertial force of the arriving eddy F_λ and the interfacial force F_σ. The balance of disruptive and cohesive forces is generally expressed in terms of the dimensionless Weber number. A critical Weber number $\mathrm{We}_{\mathrm{crit}}$ will exist at the point where cohesive and disruptive forces become balanced under a maximum stable bubble size $d_{\max}$,

$$\mathrm{We}_{\mathrm{crit}} = F_\lambda / F_\sigma = u_\lambda^2 \rho_{\mathrm{L}} d_{\max} / \sigma \tag{6}$$

Assuming that the isotropic turbulence is at least on the length scale of bubbles,[9] the turbulent velocity u_λ of an eddy of size λ in the inertial subrange can be expressed as

$$u_\lambda^2 = 2(\varepsilon\lambda)^{2/3} \tag{7}$$

Only those eddies with the length scale smaller than or equal to the bubble diameter can induce the bubble breakage,

and the larger eddies can merely transport the bubbles. For the same reason, only those bubbles with the diameters smaller than the length scale of the eddy can be formed. At the point of We_{crit} that exists, the critical eddy size λ_{crit} can be expressed as

$$\lambda_{crit} = d_{max} \tag{8}$$

From Eqs. 6–8, the following equation can be obtained[10]

$$d_{max} = \left(\frac{We_{crit}}{2}\right)^{3/5}\left(\frac{\sigma}{\rho_L}\right)^{3/5}\varepsilon^{-2/5} \tag{9}$$

The expression in Eq. 9 agrees with the equation developed by Lehr et al.,[11] except for the coefficient $(We_{crit}/2)^{3/5}$. The coefficient reflects the intrinsic of bubble-eddy system and is usually assumed as a constant. However, in our research, the ratio of liquid height to tray diameter is less than 1, bubbles cannot be fully developed, and the actual maximum bubble diameter does not agree well with the maximum stable bubble diameter as expressed in Eq. 9. Therefore, the coefficient $(We_{crit}/2)^{3/5}$ should be regarded as an adjustable parameter, and determined according to the real observations.

For the valve tray, the actual d_{max} is expressed by inducing Eq. 5 into Eq. 9:

$$d_{max} = \left(\frac{We_{crit}}{2}\right)^{3/5}\left(\frac{\sigma}{\rho_L}\right)^{3/5}\rho_G^{1/5}\left(\frac{nlh}{A_b}\right)^{-2C_2/5}(C_1 Fg)^{-2/5} \tag{10}$$

where

$$F = u_G\sqrt{\rho_G}\,. \tag{11}$$

Meanwhile, knowledge of average bubble size is of more importance than d_{max} in the industrial applications, since the former is based on the size distribution of all bubbles and generally obtained by the method of statistical averaging, rather than a single measurement. The most important statistical measurement reported in the literature is the Sauter mean bubble diameter, d_{32}, that indicates the ratio of bubble volume to the surface area for a sample of N bubbles, and is defined as follows

$$d_{32} = \frac{\sum_{i=1}^{N} d_i^3}{\sum_{i=1}^{N} d_i^2} \tag{12}$$

There is a linear relationship between d_{32} and d_{max}. Heskrth et al. assumed that these bubble size data fit a log normal distribution.[10] Thus, the coefficient between d_{32} and d_{max} could be expressed as a function of geometric mean standard deviation, and the average value of the coefficient is approximately a constant for a wide range of systems. Hence, we have

$$d_{32} = C_n d_{max} \tag{13}$$

On knowing the average size of bubbles, d_{32}, the volumetric mass transfer area a in the unit of m^2/m^3 can thus be directly correlated to the gas hold up ϕ_G,

$$a = \frac{6\phi_G}{d_{32}} \tag{14}$$

where

$$\phi_G = \frac{h_f - h_L}{h_f} \tag{15}$$

Introducing Eqs. 10 and 13 into Eq. 14, a can be expressed as

$$a = \frac{6}{C_n}C_1^{2/5}\left(\frac{We_{crit}}{2}\right)^{-3/5}\phi_G\left(\frac{nlh}{A_b}\right)^{2C_2/5}\left(\frac{\rho_L^3 g^2 F^2}{\rho_G \sigma^3}\right)^{1/5} \tag{16}$$

It is more convenient to use the dimensionless interfacial area per tray area, a', for the evaluation of tray performance. Since the gas-liquid mixed volume on the tray is generally the product of tray area and froth height, the relationship between a' and a can therefore be expressed as

$$a' = a * h_f \tag{17}$$

From Eqs. 15–17, the expression of a' can be obtained as

$$a' = \beta\left(\frac{nlh}{A_b}\right)^{\frac{2C_2}{5}}\frac{h_L\phi_G}{(1-\phi_G)}\left(\frac{\rho_L^3 g^2 F^2}{\rho_G \sigma^3}\right)^{1/5} \tag{18}$$

where

$$\beta = \frac{6C_1^{2/5}}{C_n(We_{crit}/2)^{3/5}}\,. \tag{19}$$

Experimental Section

Pure oxygen desorption method for the determination of interfacial area

Various techniques have been developed to determine the interfacial area of a tray, such as local probes,[12] photography,[13] ultrasonic attenuation,[14] and chemical methods.[15] However, since the bubble size around the valve is not homogeneously distributed, and dependent on the valve geometry, the physical methods as mentioned above are quite hard to provide precise values for the global interfacial area due to the fact that only local observations can be obtained using these methods. Therefore, the global interfacial area, as conveniently used in industrial design, has to be obtained using the chemical methods. In the present work, the pure oxygen desorption method,[16] contrary to the absorption method,[17] is employed to determine the global interfacial area. The oxygen desorption method in the work is a steady state measurement of oxygen, but not the dynamic oxygen desorption.

The oxygen transfer in water, i.e., the increasing of the oxygen concentration with respect to the time, is controlled by the liquid phase and described by an equation of the first order,

$$\frac{dc}{dt} = k_L a(c^* - c_t) \tag{20}$$

where c^* is the oxygen saturation concentration under process conditions, and c_t is the oxygen concentration at time t. The solution of this differential equation shows the course of the oxygen concentration (g/m^3) in water with time up to the saturation concentration,

$$c_t = c^* - (c^* - c_0)e^{-k_L a\Delta t} \tag{21}$$

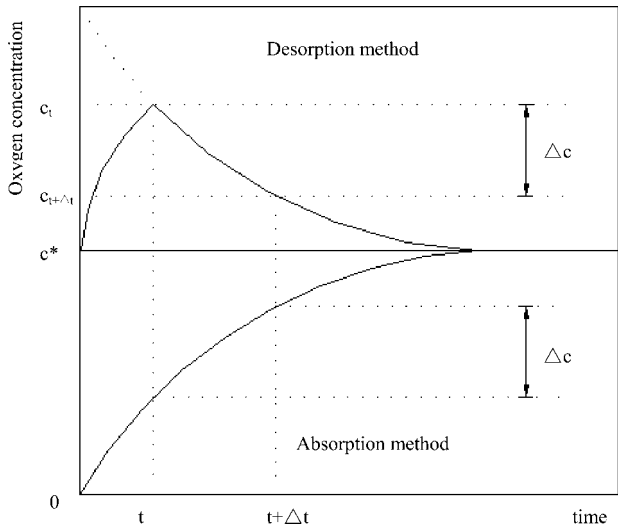

Figure 1. Comparison between the absorption method and the pure oxygen desorption method.

where c_0 is the oxygen concentration at time $t_0 = 0$, and $\Delta t(= t - t_0)$ is the residence time of the liquid. In the same way, the reduction of an excess oxygen concentration with time down to the saturation concentration can be also described using Eq. 21. The relative roles of the oxygen absorption and desorption methods are graphically illustrated in Figure 1 for easy understanding. In comparison to the absorption method with sodium sulfite, the pure oxygen desorption method is a simple and cost-effective method. With the aid of the oxygen desorption method, the tray performance can be characterized with the Murphree liquid efficiency. Substituting Eq. 21 into the traditional definition of Murphree liquid point efficiency (E_{ML}) leads to Eq. 22,

$$E_{ML} = \frac{c_t - c_{(t+\Delta t)}}{(c_t - c*)} = 1 - e^{-k_L a \Delta t} \tag{22}$$

where c_t is the inlet oxygen concentration, and $c_{(t+\Delta t)}$ is the outlet oxygen concentration.

The liquid flow pattern plays an important role in the overall tray efficiency. To evaluate the effect of valve geometry on the interfacial area, the influence of liquid flow pattern should be separated or eliminated. Therefore, ideal deflectors like the meridians of the globe are arranged on the tray and lengthened to achieve a "full-guide" liquid flow from the inlet to the overflow weir. The ideal deflectors are expected to completely divide the tray surface into several individual channels. Coming from the inlet, the liquid is evenly guided into these channels, and the liquid vortex and backflow were almost eliminated. Thus plug flow, an ideal flow pattern, was roughly approached, as having been proved in our previous work.[18] Owing to the plug liquid flow being realized on the tray, the liquid residence time Δt can thus be expressed as

$$\Delta t = \frac{A_b h_f \ (1 - \phi_G)}{V_L} \tag{23}$$

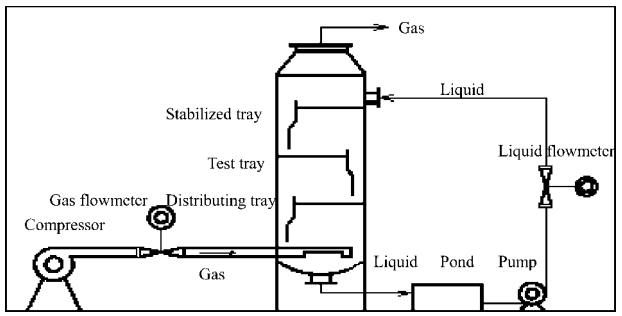

Figure 2. Experimental apparatus.

From Eqs. 17, 22, and 23, a' can be written as

$$a' = -\frac{V_L}{k_L A_b (1 - \phi_G)} \ln\left(1 - \frac{c_t - c_{(t+\Delta t)}}{c_t - c^*}\right) \tag{24}$$

The experimental values of a' calculated from Eq. 24 can be substituted into Eq. 18 to determine the coefficients of β and C_2.

Apparatus and procedure

A schematic diagram of the experimental apparatus[19] is shown in Figure 2. Three identical trays were placed in a column with a diameter of 1 m. The middle tray was served as a test tray, whereas the upper tray was functionalized as a stabilized tray, and the bottom one played the role of vapor distribution. The space between the adjacent trays was 0.5 m. The tray structural parameters were as follows: weir length of 0.85 m, weir height of 0.03 m, tray bubble area of 0.687 m^2, and perforation (the ratio of perforation area to tray area) of 11.4%. Four ideal deflectors were placed on the trays for distributing and regulating the liquid flow, so as to form a plug-flow pattern.[18]

Three types of valves, Glitsch V-1 valve (V1), rhombic valve (RV), and double rhombic valve (DRV), as shown in Figure 3, were equipped and tested. The RV and DRV valves were invented and developed in our lab. The detailed geometry values of the three valves are listed in Table 1. Under the working condition of the test column as shown in Figure 2, the slot heights of all three valves are fixed and equal to the maximum valve lift height of 8.5 mm. Since the slot height h mainly controls the weeping point, such a selection of h values leads to the weeping being almost zero. The effective slot perimeter l was obtained by subtracting the valve leg width from the valve land perimeter. Statistically, the effective slot perimeter per tray area, l, of RV was 9.19% larger

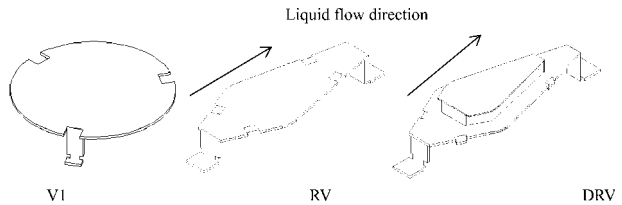

Figure 3. Configurations of V1, RV, and DRV.

Table 1. Valve Geometry Parameters

Parameters	n	l (mm)	h (mm)
Valves			
V1	75	136	8.5
RV	58	192	
DRV	45	302	

than that of V1, whereas the l value of DRV was 33.20% higher than that of V1. The DRV valve was specially designed by adding a small-scale valve right on the main rhombic valve sheet in order to intensify its performance.

Air/water at 25°C and atmospheric pressure were taken as the test system, with a gas volume rate ranging from 0.14 to 0.29 m^3/s and a liquid volume rate from 1.1×10^{-3} to 9.7×10^{-3} m^3/s. The ratio of air to water flow rates was appropriately adjusted to ensure the operability of the test column. The gas volume rate was measured with a probe flowmeter of type SY-93 manufactured by EPI Company, USA, (measured precision ±1.5% FS) while a smart vortex flowmeter 8800C supplied by Fisher-Rosemount Co. was used for the determination of liquid rate (measured precision ±0.1% FS). The high excess concentration was obtained by feeding pure oxygen continuously into the water source. Enough time was required to let oxygen dissolve sufficiently into the water source so that an oxygen concentration of about 20 g/m^3 was reached. As the oxygen-rich water being pumped to flow through the trays, the oxygen concentration in the clean water decreased toward the oxygen saturation concentration by the stripping of the excess oxygen. When the operating column reached steady state, which was about twenty minutes later since the start of the experiment, liquid samples were collected from the inlet and outlet of the test tray. The samples were titrated by iodometry[20] without delay to determine the oxygen concentrations. The clear liquid heights at different locations of the test tray were measured using a series of U-tube differential manometers, and the froth height was obtained using a ruler placed directly on the tray. The measurements of both clear liquid and froth heights were accurate to mm, and schematically illustrated in Figure 4. The experimental values of froth porosity, ϕ_G, were calculated using Eq. 15.

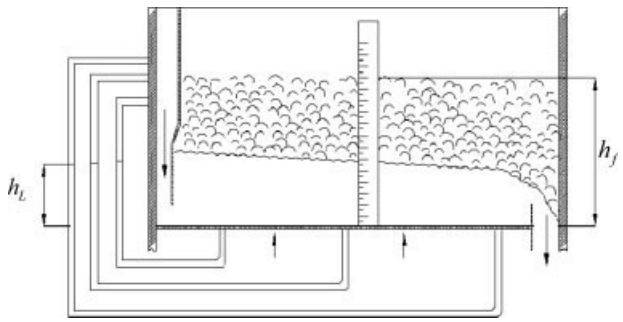

Figure 4. Measurements of the clear liquid height (h_L) and froth height (h_f) on the tray.

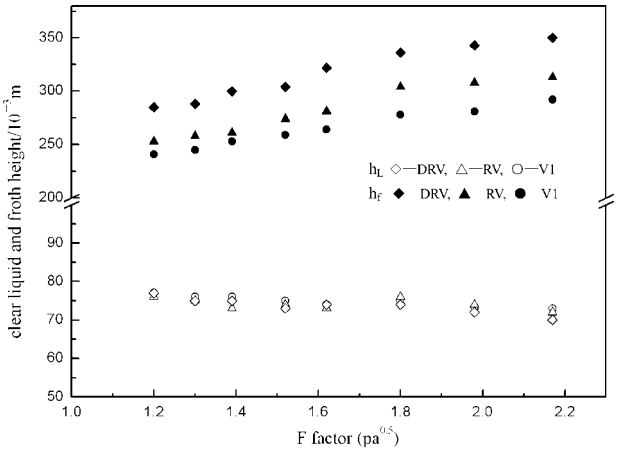

Figure 5. Clear liquid height (h_L) and froth height (h_f) as a function of *F*-factor.

Results and Discussion

Froth porosity

Froth porosity, one of the most important parameters, has been involved in many research papers. In the present work, the clear liquid height and froth height were experimentally determined to calculate the froth porosity using Eq. 15. The experimental values of the clear liquid height h_L for all the three kinds of valve trays are found to be almost the same, as shown in Figure 5. This is consistent with most conclusions drawn by other researchers in literature.[21] At the working condition of negligible weeping and entrainment, h_L is determined by weir height and liquid volume rate, as shown in Figure 6. The following correlation, referred from the literature,[21] is appropriate for three types of valve trays

$$h_L = H_w + 1.11\left(\frac{V_L}{B_w}\right)^{2/3} \tag{25}$$

where V_L is the liquid volume rate, and B_W denotes the weir width. The froth height is mainly affected by the valve geometry and gas velocity, as shown in Figures 5 and 6. When

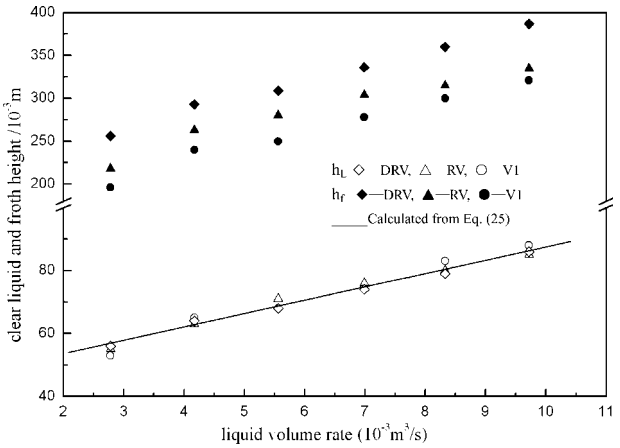

Figure 6. Clear liquid height (h_L) and froth height (h_f) as a function of liquid volume rate (V_L).

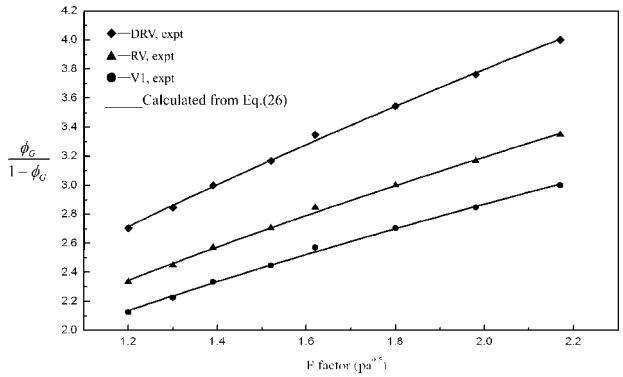

Figure 7. $\phi_G/(1-\phi_G)$ values as a function of *F*-factor.

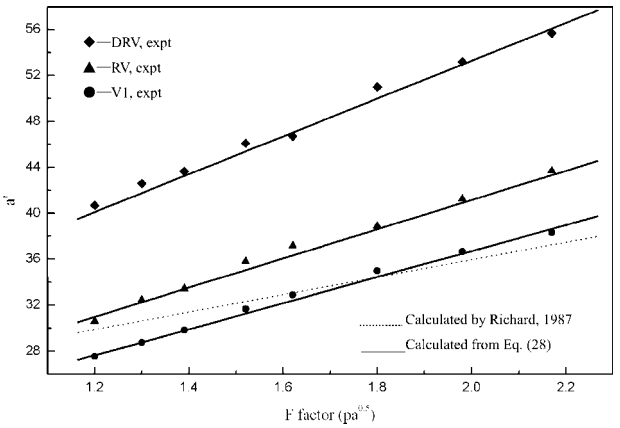

Figure 9. Interfacial area per tray area (a') as a function of *F*-factor.

the valve tray has a longer effective valve perimeter, l, the gas velocity through the slot will decrease, and the gas can be more homogeneously distributed, resulting in an increase of the froth height. The $\frac{\phi_G}{1-\phi_G}$ values in Eq. 18 as a function of F-factor, as presented in Figure 7, have almost the same tendency as the froth height. Since $\frac{\phi_G}{1-\phi_G}$, as shown in Figure 8, is only a very weak function of the liquid volume rate and kept almost constant, the liquid volume rate is regarded to be of negligible influence. Therefore, a regressive correlation of $\frac{\phi_G}{1-\phi_G}$ for the valve tray is recommended as follows

$$\frac{\phi_G}{1-\phi_G} = 12.23^{\pm 0.61}\left(\frac{nlh}{A_b}\right)^{0.90^{\pm 0.18}} F^{0.61^{\pm 0.05}} \qquad (26)$$

Interfacial area per tray area a′

Interfacial area a' was calculated from Eq. 24 using the pure oxygen desorption experimental data. The liquid film coefficient k_L of oxygen transfer was evaluated according to the correlation recommended by Linek et al.[22] This correlation is deduced based on the "eddy" model, assuming that the small scales of turbulent motion affect the mass transfer. In any case, these turbulent motions are much smaller in scale than gas bubbles. As a result, the size of the gas bubbles is not a critical parameter for the estimation of k_L. Since the tray configurations, including the valve geometry, mainly affects the bubbles' size, the influence of these motions on k_L can therefore be neglected. The similar conclusion by Richard et al.[1] also indicated that the mass transfer coefficient was not a strong function of tray type but the interfacial area was. As shown in Figures 9 and 10, the greater interfacial area a' was obtained due to the longer effective perimeter l. Statistically, comparing to the case of V1, a' of RV is about 12.49% higher, and that of DRV is 45.64% higher.

To determine the parameters of β and C_2 in Eq. 18 an assumption of linear relationship between ε and nlh/A_b in Eq. 5 is at the first thought made and tried to simplify the optimization. This assumption means that $C_2 = 1$ and the parameter β can be easily and directly calculated from the experimental values of a' using Eq. 18. The calculations indicate that the calculated β changes very little with the valve geometry. As illustrated in Figure 11, all the three types of valves, V1, RV, and DRV, have nearly the same β values, which implies that the assumption made above is reasonable and of great simplicity.

Moreover, Figure 11 also demonstrates that β decreases with the increasing F factor and depends quite weakly on the

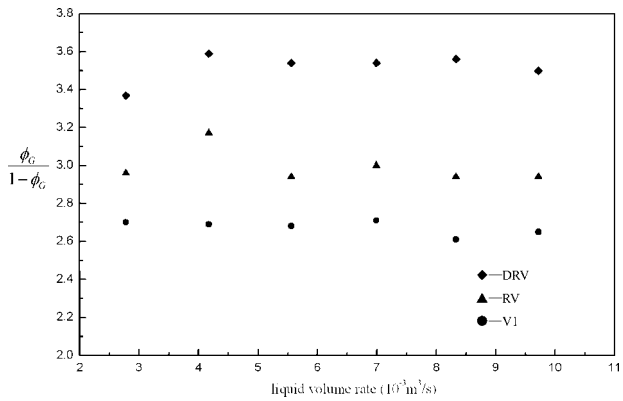

Figure 8. $\phi_G/(1-\phi_G)$ values as a function of liquid volume rate.

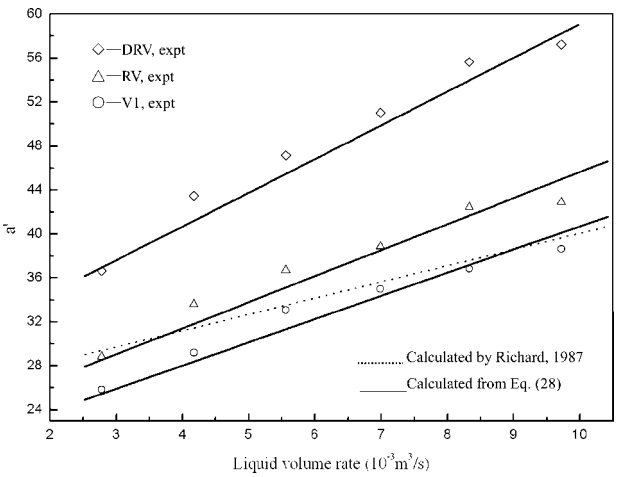

Figure 10. Interfacial area per tray area (a') as a function of liquid volume rate (V_L).

liquid flow rate. Even though β is the function of C_1, C_n, and We_{crit}, as shown in Eq. 19, C_n and We_{crit} usually behave to be constants, or of small deviations as pointed out in most papers.[23,24] Therefore, the decreasing β with the increasing F has to be attributed to the dependence of C_1 on F. Since C_1 indicates the efficiency of energy exchange between the gas and liquid, the dependence of C_1 on F-factor can be explained from the gas–liquid contact time. When the superficial gas velocity is raised, the liquid height changes little, as shown in Figure 5, and the contact time decreases accordingly. The decreasing contact time causes the reduction of energy exchange between the gas and liquid, resulting in the decrease of C_1 and β. As for the influence of the liquid volume rate on C_1 and β, there are two existing factors that are opposite to each other: the enhanced liquid height with the increasing liquid volume rate, as shown in Figure 6, provides longer time for the vapor passing through the liquid in the vertical direction, whereas the contact time in the horizontal direction decreases with the increasing superficial liquid velocity. The positive and negative effects of the liquid flow rate on the contact time neutralize each other, so that the energy dissipation per liquid mass changes very little with the liquid flow rate. According to the analysis above, β is just regarded as a function of the F-factor within the limit $2.0 \times 10^{-3} \leq L \leq 10.0 \times 10^{-3}$ m^3/s, and the regressive expression of β can be obtained as

$$\beta = 0.5313^{\pm 0.0134} F^{-0.44^{\pm 0.03}} \tag{27}$$

Combining Eqs. 25–27 with 18, the regression equation of a' can be finally expressed as

$$a' = 6.50^{\pm 0.81} \left(\frac{nlh}{A_b}\right)^{1.3^{\pm 0.19}} \left[H_w + 1.11\left(\frac{V_L}{B_w}\right)^{2/3}\right] \times \left(\frac{\rho_L^3 g^2}{\rho_G \sigma^3}\right)^{1/5} F^{0.57^{\pm 0.03}} \tag{28}$$

The experimental interfacial areas of all three valves (V1, RV, and DRV) in this study, as well as the experimental data of V1 valve by Richard et al.,[1] are used to examine the accuracy and applicability of Eq. 28. The calculation results,

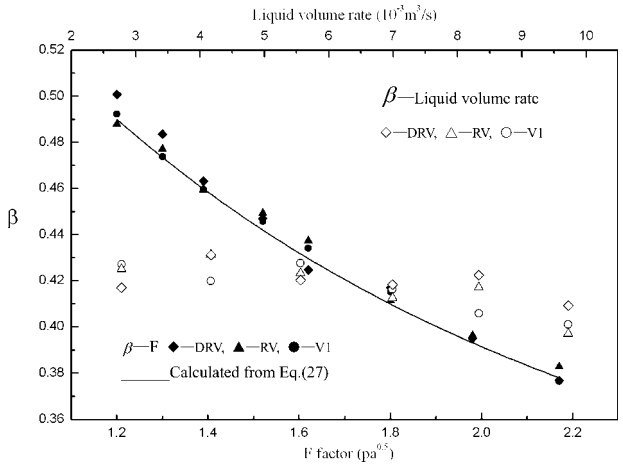

Figure 11. β values as a function of F-factors and liquid volume rate (when $C_2 = 1$).

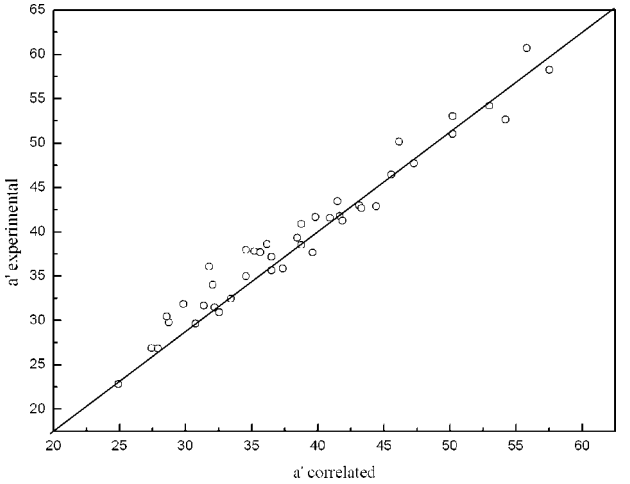

Figure 12. Comparison between the experimental and correlated (Eq. 28) interfacial areas per tray area.

as given in Figures 9, 10, and 12, indicate that Eq. 28 fits the data from Richard et al.[1] with a mean deviation of 8.28%, and represents the experimental data of all three valves in this study with a mean deviation of 1.22%. The comparison between the correlated and experimental interfacial areas, as more clearly shown in Figure 12, justifies Eq. 28 to be an excellent correlation.

Conclusions

The mechanism of interface formation is explored in this article based on the Kolmogoroff's isotropic turbulence theory, and a mathematical model is developed to predict the interfacial area of the valve tray. The incorporation of the isotropic turbulence theory enables the model to be simple and convenient for applications.

Experiments are carried out to compare the interfacial areas of V1, RV, and DRV. The results show that the vale geometry is the main factor affecting the energy dissipation rate and the froth porosity, and thus finally influencing on the interfacial area. The interfacial area on the tray is also found to increase with the increasing effective valve perimeter per tray area. All the above experimental phenomena can be described well with the model developed in the article.

The most important characteristic of present model is to correlate the interfacial area with the valve geometry. This correlation is expected to provide a wide range of use in the calculations of interfacial area for the valve trays that have different valve geometries.

Acknowledgments

The authors are grateful for the financial support from National 985 Project of China and the National Natural Science Foundation of China (No. 20576050).

Notation

a = interfacial area density (/m)
a' = interfacial area per tray area (dimensionless)

A_b = bubble area (m^2)
B_w = weir width (m)
c = oxygen concentration (g/m^3)
C_1, C_2 = regression coefficients (dimensionless)
d = bubble diameter (m)
ΔE_L = energy dissipation rate per tray area (J/m^2 s)
E_{ML} = Murphree liquid tray efficiency (dimensionless)
F = F-factor, product of superficial gas velocity and square root of gas mass density, $pa^{0.5}$
h = slot height (mm)
h_f = froth height (m)
h_L = clear liquid height (m)
H_w = weir height (m)
k_L = liquid-side mass transfer coefficient (m/s)
l = effective slot perimeter per valve (mm)
n = valve number per tray (dimensionless)
ΔP_L = gas pressure drop through liquid (Pa)
u_G = superficial gas velocity (m/s)
u_λ = turbulent velocity (m/s)
V = volume rate (m^3/s)
We = Weber number (dimensionless)

Greek letters

β = regression coefficient (dimensionless)
ε = energy dissipation rate per unit liquid mass (m^2/s^3)
λ = length scale of an eddy (m)
ϕ_G = gas hold up (dimensionless)
ρ = density (kg/m^3)
σ = surface tension (N/m)

Subscript

crit = critical
32 = Sauter mean
max = maximum stable
L = liquid
G = gas

Literature Cited

1. Scheffe RD, Weiland RH. Mass-transfer characteristics of valve trays. *Ind Eng Chem Res*. 1987;26:228–236.
2. Hibikia T, Ishiic M. Interfacial area concentration of bubbly flow systems. *Chem Eng Sci*. 2002;57:3967–3977.
3. Kocamustafaogullari G, Huang WD, Razi J. Measurement of modeling of average void fraction, bubble size and interfacial area. *Nucl Eng Des*. 1994;148:437–453.
4. Millies M, Mewes D. Interfacial area density in bubbly flow. *Chem Eng Process*. 1999;38:307–319.
5. Kolmogoroff AN. On the disintegration of drops in turbulent flow. *Dokl Akad Nauk SSSR*. 1949;66:825–829.
6. Luo H, Svendsen HF. Theoretical model for drop and bubble breakup in turbulent dispersions. *AIChE J*. 1996;42:1225–1233.
7. Liang YC, Zhou Z, Wu YT, Geng J, Zhang ZB. A nonequilibrium model for distillation processes. *AIChE J*. 2006;52:4229–4239.
8. Liu CJ, Yuan XG, Yu KT, Zhu XJ. A fluid-dynamic model for flow pattern on a distillation tray. *Chem Eng Sci*. 2000;55:2287–2294.
9. Prince MJ, Blanch HW. Bubble coalescence and break-up in air-sparged bubble columns. *AIChE J*. 1990;36:1485–1499.
10. Hesketh RP, Russell TWF. Bubble size in horizontal pipelines. *AIChE J*. 1987;33:663–667.
11. Lehr F, Mewes D. A transport equation for the interfacial area density applied to bubble columns. *Chem Eng Sci*. 2001;56:1159–1166.
12. Zhao D, Guo L, Lin C, Zhang X. An experimental study on local interfacial area concentration using a double-sensor probe. *Int J Heat Mass Transf*. 2005;48:1926–1935.
13. Pohorecki R, Moniuk W, Bielski P, Sobieszuk P, Dąbrowiecki G. Bubble diameter correlation via numerical experiment. *Chem Eng J*. 2005;113:35–39.
14. Delhaye JM, Brichard P. Interfacial area in bubbly flow: experimental data and correlation. *Nucl Eng Des*. 1994;151:65–77.
15. Tomida T, Yusa F, Akazaki T. Effective interfacial are and liquid-side mass transfer coefficient in upward two-phase flow of gas-liquid mixtures. *Chem Eng J*. 1978;16:81–88.
16. Martin R, Wagner H, Pöpel J, Kalte P. Pure oxygen desorption method- a new and cost-effective method for the determination of oxygen transfer rates in clean water. *Wat Sci Tech*. 1998;38:103–109.
17. Puskeiler R, Weuster-Botz D. Combined sulfite method for the measurement of the oxygen transfer coefficient k_La in bioreactors. *J Biotechnol*. 2005;120:430–438.
18. Zhou Z, Liang YC, Zhang ZB. New method for design an energy-saving and its hydrodynamic aspects: temperature distribution and efficiency of deflected tray-95. *Ind Eng Chem Res*. 2003;42:2219–2222.
19. Zhang ZB, Meng WM, Zhou Z, Liang YC, Wu YT. The superior aspects of the arc downcomer tray with total deflectors, conference of separations technology VI: new perspectives on very large-scale operations, Kingfisher Resort, Fraser Island, Queensland, Australia, 2004.
20. Meites L. *Handbook of Analytical Chemistry*, 1st ed. New York: McGraw-Hill, 1964.
21. Wang SH. *Petrochemical Engineering Design Handbook*, Beijing: Chemical Industry Publishing Company, 2002.
22. Linek V, Kordac M, Moucha T. Mechanism of mass transfer from bubbles in dispersions Part II: Mass transfer coefficients in stirred gas-liquid reactor and bubble column. *Chem Eng Process*. 2005;44:121–130.
23. Hesketh RP, Etchells AW, Russell TW. Bubble breakage in pipeline flow. *Chem Eng Sci*. 1991;46:1–9.
24. Rigby GD, Evans GM, Jameson GJ. Bubble breakup from ventilated cavities in multiphase reactors. *Chem Eng Sci*. 1997;52:3677–3684.

Manuscript received Mar. 9, 2007, and revision received Jan. 19, 2008.